RADIO SCIENCE, VOL. 43, RS6008, doi:10.1029/2007RS003769, 2008

A comprehensive evaluation of the errors inherent in the use of a two-dimensional shell for modeling the ionosphere

Dru A. Smith,[1] Eduardo A. Araujo-Pradere,[2,3] Cliff Minter,[2,3] and Tim Fuller-Rowell[2,3]

Received 7 November 2007; revised 24 July 2008; accepted 22 October 2008; published 27 December 2008.

[1] Accurately modeling the ionosphere is a critical component to many radionavigation applications. However, in a significant number of cases, these models assume the ionosphere is compacted into a thin shell surrounding the Earth, rather than a full three-dimensional field. While such models allow for ease of use and small storage needs, they are necessarily lacking in detailed information on the actual three-dimensional distribution of electrons in the ionosphere. This paper attempts to quantify all geometric and numerical errors made through the use of a shell model. Such errors can reach as high as 14% on days of no strong ionosphere activity. Ultimately, this paper concludes that the highest levels of accuracy require the total electron content of the ionosphere be modeled three-dimensionally. However, for those who must continue to use a shell model, a new mapping function has been derived which removes as much as 50% of the total errors seen using the previous, standard mapping function for shell models.

Citation: Smith, D. A., E. A. Araujo-Pradere, C. Minter, and T. Fuller-Rowell (2008), A comprehensive evaluation of the errors inherent in the use of a two-dimensional shell for modeling the ionosphere, *Radio Sci.*, *43*, RS6008, doi:10.1029/2007RS003769.

1. Introduction

[2] The ionosphere is a three-dimensional field of ions and free electrons in the upper atmosphere of the Earth which changes with time (thus is truly four-dimensional). Because the ionosphere affects the propagation of electromagnetic (EM) waves (such as those from the Global Positioning System, GPS), it has been studied and modeled for years [*Komjathy*, 1997; *Bilitza*, 2001]. The impact of the ionosphere on EM waves is directly related to the number of electrons through which the wave passes, so any useful model of the ionosphere must be able to accurately describe the total number of electrons along any ray in any direction passing through the ionosphere. This is not simple task, but is aided by the fact that the majority of electrons in the ionosphere generally are concentrated in a relatively "thin" layer. Although the ionosphere is hundreds of kilometers thick, the majority of free electrons fall in a ~100 km thick band centered around 400 km above the Earth's surface [*Bilitza*, 2001]. As such, many attempts to model the ionosphere over the years have begun with the (unrealistic, but mathematically simple) assumption that the ionosphere is a two-dimensional shell surrounding the Earth at some specific radius. This paper seeks to examine the inherent mathematic/geometric and geophysical limitations in using such a model, quantify their impact on determination of the true electron distribution along various ray paths and determine when (if at all) such shell models can be used reliably. In particular, the impact of using the 2-D ionospheric shell approximation in the presence of vertical and horizontal structure will be quantified by using a realistic assimilated ionosphere. The results of this study will show that nonnegligible errors from geometry alone occur when an infinitesimally thin shell is used, rather than a simple shell of some finite thickness. As further refinements are added, the errors suffered by a simple shell model grow, though not to the point that a shell model is useless. It is the quantification of these errors that will show that shell models can be useful for applications at certain levels of accuracy, while higher orders of accuracy must be reserved for more detailed 3-D models. This study compliments previous efforts to evaluate the effect of using an ionospheric

[1] National Geodetic Survey, National Oceanic and Atmospheric Administration, Silver Spring, Maryland, USA.
[2] Space Weather Prediction Center, National Oceanic and Atmospheric Administration, Boulder, Colorado, USA.
[3] Cooperative Institute for Research in Environmental Sciences, University of Colorado, Boulder, Colorado, USA.

0048-6604/08/2007RS003769$11.00

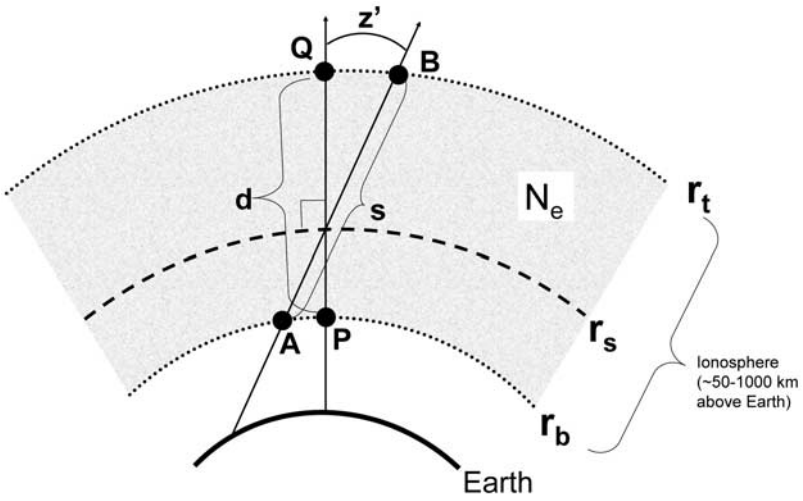

Figure 1. Idealization of the geometry inherent to the impact of the ionosphere on GPS, including a generic STEC ray (AB) and the VTEC ray (PQ).

shell model [e.g., *Radicella et al.*, 2004; *Komjathy and Langley*, 1996].

2. Total Electron Content

[3] Consider the example shown in Figure 1. The density of electrons (elec/m^3) at any point is N_e. Of interest is the total number of electrons (per square meter) passed through along the slanted path (through points A and B in Figure 1) through the ionosphere, the well known "Total Electron Content", or "TEC":

$$TEC = \int_A^B N_e ds \tag{1}$$

[4] The TEC of equation (1) will have units of elec/m^2, but is more frequently expressed in TEC Units ("TECU") of 1 TECU = 10^{16} elec/m^2. Note that there is no scientific consensus as to where the "bottom" and "top" of the ionosphere lie (they are "transitional boundaries"), but values of 50 to 1000 km above the Earth cover the majority of such estimates. Also, it should be noted that the path of the EM wave is slightly bent (refracted) as it traverses the ionosphere, but for the purposes of this study, such an effect has been ignored. Since we focus here on application to GPS systems at gigahertz frequencies, such effects are small.

[5] A variety of types of TEC will be used in this study. First is the "Slant TEC" or "STEC" which is the actual TEC along the slanted line from a point below the ionosphere to a point above it (computed from equation (1)). The distance traveled is "s" (shown as line AB in Figure 1). The formula for STEC is therefore identical to the generic TEC formula:

$$STEC = \int_A^B N_e ds \tag{2}$$

[6] The second type of TEC to be considered in this paper is called "Vertical TEC" or "VTEC", and is the special case of STEC where the EM ray travels through the ionosphere along the radial direction. The distance thus traveled will be called "d" (shown as line PQ in Figure 1). The formula for VTEC is:

$$VTEC = \int_P^Q N_e ds \tag{3}$$

where the differential distance "ds" is aligned radially on the line through points P and Q.

3. Electron Density, Geometry, and 2-D Shells

[7] The ionosphere is a highly complex field, but it does (generally) tend to have a dense central layer around 400 km above the Earth. While the approximate location of r_s in Figure 2 can be considered to lie in this dense region, the actual value of "r_s" in Figure 2 is irrelevant, as it is simply a convenient tool to introduce a piercing angle, z'. For any given slanted ray, picking a

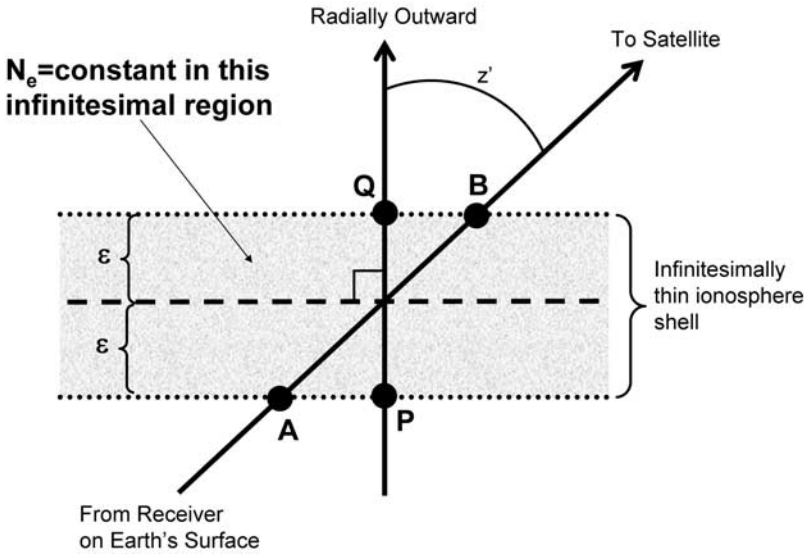

Figure 2. Geometry of an idealized planar 2-D ionosphere shell.

different r_s yields a different piercing point and piercing angle z'. The values r_s and z' will simply be used as tools for aiding in the geometric relationships derived later.

[8] Because the length of the slant ray, s, is so critical to the understanding of STEC, its exact formula should be known. Using basic spherical relationships (full derivation is found in Appendix A), one can write the equations for both s and d as:

$$s = \sqrt{r_t^2 - r_s^2 \sin^2(z')} - \sqrt{r_b^2 - r_s^2 \sin^2(z')} \quad (4)$$

$$d = r_t - r_b \quad (5)$$

[9] We will make extensive use of equation (4) throughout the next few sections. It is briefly noted that alternative formulae for equation (4) have been commonly used which depend upon the elevation angle (above the horizon) of the satellite, rather than the piercing angle of the ray through the shell. While mathematically equivalent to equation (4), the dependence on elevation angle, rather than piercing angle, means such formulae do not lend themselves easily to the analysis within this paper.

[10] Because of the dense electron layer around 400 km, modeling of the ionosphere has frequently been done by assuming that the ionosphere is not a 3-D field, but is instead compressed in the radial direction (from its top and bottom) into a 2-D "shell" located around the densest layer of the ionosphere [*Komjathy*, 1997].

[11] Such a "shell model" has many advantages, including mathematical simplicity and reduction in overall data storage (but this comes with the basic disadvantage of loss of information content, of course). After condensing to a shell the only information left over is obviously the VTEC at any given point on the shell. This is because the radial compression takes the full VTEC value along a radial line and compresses it to a point, without changing its total value. However, since most EM waves of interest (such as GPS signals) do not pass vertically through the ionosphere, but rather on a slant, some method must be chosen to derive STEC values from the still-available VTEC values. To distinguish between the actual TEC values along the slant ray (STEC), and those which are "mapped" or derived solely from VTEC information, the term "MSTEC" is introduced to mean "Mapped STEC".

[12] For many years, computing MSTEC from VTEC has been done with a simple mapping function (denoted "*W*" in this paper; the "hat" is used, to distinguish the mapping function from the actual ratio of STEC to VTEC, which will be designated later as simply "W"):

$$MSTEC(\vec{X}_{sat}, \vec{X}_{rec}) = \hat{W} \times VTEC(\vec{X}_{pp}) \quad (6)$$

where $\mathbf{X}_{sat}$ is the 3-D coordinate vector for a satellite (such as some GNSS satellite giving off a radio signal), $\mathbf{X}_{rec}$ is the 3-D coordinate vector of the receiver on Earth's surface (receiving the radio signal), and $\mathbf{X}_{pp}$ is the 3-D coordinate vector of the pierce point where the line from receiver to satellite pierces the 2-D ionosphere shell. The coordinates of the pierce point are usually

expressed only in latitude and longitude, since the shell's location is at a constant (given) height. Also, the pierce point coordinate vector can be expressed as a function of the satellite and receiver coordinates and the shell radius:

$$\vec{X}_{pp} = \vec{X}_{pp}(\vec{X}_{sat}, \vec{X}_{rec}, r_s) \tag{7}$$

[13] Finally, the most common, by far, mapping function used in most of books and papers on this subject seems to be:

$$\hat{W} = \frac{1}{\cos(z')} \tag{8}$$

where z' (introduced earlier) is the angle made between the radially outward direction and the direction of the slant line between the satellite and receiver (see Figure 1 for a reminder). As such, it is a function of the shell's location, and the location of the satellite and receiver:

$$z' = z'(\vec{X}_{sat}, \vec{X}_{rec}, r_s) \tag{9}$$

[14] In similar fashion to equation (4), there are alternative formulae for equation (8) in the literature which depend on the elevation angle of the ray above the horizon, rather than the piercing angle through a shell. Those alternative formulae are less useful for this analysis and are not presented here.

[15] So finally one often sees (eliminating unnecessary variables):

$$MSTEC = \frac{VTEC}{\cos(z')} \tag{10}$$

where we compute MSTEC, an approximated (or "mapped") STEC, rather than the true STEC. Note the dependence on z' in equation (10), and the dependence which z' has on r_s from equation (9). As such, using the mapping function of equation (8), one can see that the value of MSTEC depends upon the chosen shell height, even though VTEC remains the same for all shell heights.

[16] There are well known (and not so well known) inherent errors associated with using this mapping function. The most obvious (though not comprehensively studied) is that deriving MSTEC from VTEC at a single point yields no actual information about the total electron content along the actual slant path (STEC); that is, all ionosphere information about the ionosphere along a slanted path is expected to be contained at one point (the piercing point) in the shell. The errors inherent in this approximation are the primary focus of this paper. However, a second (and less studied) error is that the simple mapping function of equation (10) fails to address the curvature of the precondensed (3-D) ionosphere, and thus will always suffer from a systematic error from a purely geometric standpoint. (It will be shown later that the curvature of the postcondensed (2-D) ionosphere shell will not be a factor in this discussion.) All of these geometrical issues will be addressed in the next section prior to analyzing the actual ionosphere data itself.

4. Mapping Function ($\hat{W}$) Versus the True STEC/VTEC Ratio (W)

[17] The need for a mapping function arises when VTEC is given, STEC is needed, and thus MSTEC is computed as an estimate to STEC. It will be instructive for the following discussion to derive the best mapping function between MSTEC and VTEC under certain simplified geometric situations. First, it is critical to recall the distinction between the mapping function ($\hat{W}$) of equation (6) and the actual ratio between STEC and VTEC, which is designated "W" (without the hat):

$$W = STEC/VTEC \tag{11}$$

The obvious idea behind choosing a mapping function is to find a $\hat{W}$ value that best represents the actual W value. This will be pursued in the next few sections.

5. Flat-Plane Mapping Function

[18] Consider (for the moment) the ionosphere condensed to an infinitesimally thin (but with finite thickness) layer with no curvature. Because the thickness of this layer is not zero, it will be referred to as a "nearly flat plane", to distinguish it from a "flat plane" which would have zero thickness. (The term "flat" will be used to mean "zero thickness" through the next few sections.)

[19] This nearly flat plane contains electrons at a density N_e, as shown in Figure 2. Under such a scenario, all electrons have been condensed to a constant value in an infinitesimally local area and as such, the STEC and VTEC values (subscripted "nfp" for "nearly flat plane") for such a model are:

$$\begin{aligned} STEC_{nfp} &= s_{nfp} \times N_e = \overline{AB} \times N_e \\ VTEC_{nfp} &= d_{nfp} \times N_e = \overline{PQ} \times N_e \end{aligned} \tag{12}$$

where the values "s" and "d" are the slant (AB) and vertical (PQ) lengths of interest as before (but now compressed to their infinitesimally small values). Rearranging equation (12), and removing N_e yields:

$$STEC_{nfp} = \frac{s_{nfp}}{d_{nfp}} \times VTEC_{nfp} \tag{13}$$

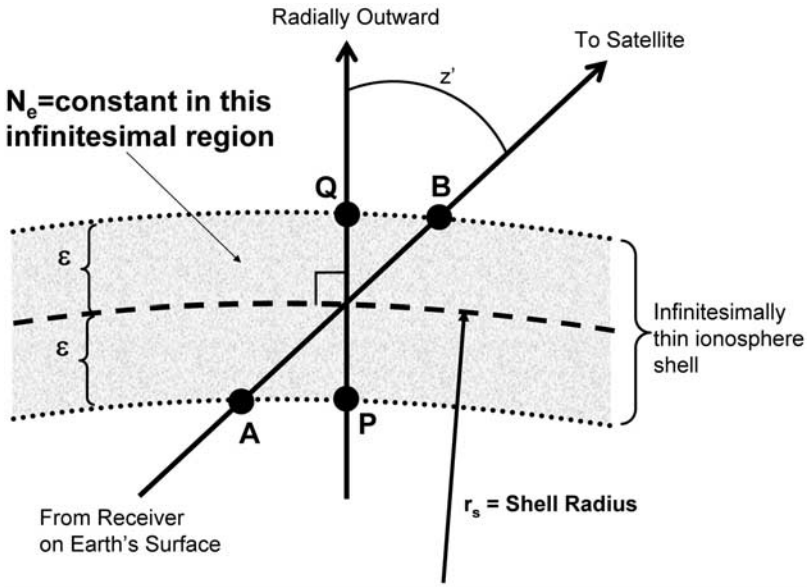

Figure 3. Geometry of an idealized spherical 2-D ionosphere shell.

Examining equation (13) in combination with equation (11), one sees that the mapping function in a nearly flat plane geometry is:

$$W_{nfp} = \frac{s_{nfp}}{d_{nfp}} \tag{14}$$

The relationship between s and d under the flat shell geometry is a trivial cosine relationship which may be inferred directly from the geometry of Figure 2. Combining that with equation (14), one can arrive at:

$$\frac{s_{nfp}}{d_{nfp}} = \frac{1}{\cos(z')} = W_{nfp} \tag{15}$$

One final step must be taken before one can arrive at the actual mapping function between STEC and VTEC in planar geometry. Remember that equation (15) was derived for a nearly flat plane of small, but finite, thickness, "d". To derive the mapping function between STEC and VTEC in an actual two-dimensionally flat planar geometry, the limit as d approaches zero must be taken (where the subscript "fp" is for a truly two-dimensional "flat plane", in contrast to the "nfp" subscript used up to this point):

$$W_{fp} = \underset{d_{nfp}->0}{Lim}\,(W_{nfp}) = \underset{d_{nfp}->0}{Lim}\,\frac{s_{nfp}}{d_{nfp}} = \frac{1}{\cos(z')} \tag{16}$$

(Although the limit in equation (16) seems trivial, it is necessary in order to draw a parallel with the next example.) Equation (16) shows that, under an actual two-dimensional flat plane ionosphere, the well known mapping function of equation (8) is exact.

6. Spherical Shell Mapping Function

[20] Now, consider the same condensed ionosphere as before, but of spherical shape (see Figure 3). As before, the STEC and VTEC values can be directly related to infinitesimal lengths through the shell and a constant local N_e value at the pierce point. That is, equations (12), (13), and (14) still hold (where the subscript "nfp" may be replaced with "nfs" for "nearly flat shell"), even in the spherical domain.

[21] However, the nonplanar nature of the shell changes the relationship between s and d from that of equation (15) to something much more complex. Using equation (4), and substituting $r_s - (d/2)$ for r_b and $r_s + (d/2)$ for r_t, the mapping function for a nearly flat shell (which is also the ratio s/d for a thin shell of thickness "d" centered around radius "r_s"), can be written:

$$W_{nfs} = \frac{s_{nfs}}{d_{nfs}} = \frac{1}{d_{nfs}}\left[\sqrt{\left(r_s + \frac{d_{nfs}}{2}\right)^2 - r_s \sin^2 z'} - \sqrt{\left(r_s - \frac{d_{nfs}}{2}\right)^2 - r_s \sin^2 z'}\right] \tag{17}$$

[22] Through a series expansion (of equation (17)) about d_{nfs}, one can immediately see that equations (17) and (15) share the same cosine relationship:

$$W_{nfs} = \frac{s_{nfs}}{d_{nfs}} = \frac{1}{\cos(z')} + \frac{\cos^2(z') - 1}{8r_s^2 \cos^5(z')} d_{nfs}^2 + \frac{7 - 10\cos^2(z') + 3\cos^4(z')}{128 r_s^4 \cos^9(z')} d_{nfs}^4 + \ldots \quad (18)$$

[23] At first glance, equation (18) would seem to imply that a set of second (or even fourth) order terms should be applied to the spherical mapping function. However, as before, notice that equation (18) holds for the geometry of a shell whose thickness (d_{nfs}) is small, but still finite. So, as before, the limit as the thickness approaches zero must be taken to arrive at the actual mapping function in this geometry:

$$W_{fs} = \lim_{d_{nfs} \to 0} (W_{nfs}) = \lim_{d_{nfs} \to 0} \frac{s_{nfs}}{d_{nfs}} = \frac{1}{\cos(z')} \quad (19)$$

[24] Notice in equation (19) that the geometry remains spherical (that is, r_s remains a finite number.) This means that a truly zero-thickness shell of spherical shape has the same mapping function as that of a flat plane and thus the spherical nature of the postcondensed ionosphere has no impact on the mapping function.

[25] However, the second (and higher) order terms in equation (18) indicate that some content in the mapping between VTEC and STEC is being overlooked in a spherical ionosphere of nonzero thickness. This gets to the shape of the precondensed ionosphere, discussed in the next session.

7. Errors From Precondensed Spherical Geometry

[26] As pointed out in the previous section, if the ionosphere were truly a two-dimensional spherical shell (when approached as a limit), then the relationship between STEC and VTEC (the mapping function) exactly matches that of flat-plane geometry (equations (19) and (16) match). However, we know that the ionosphere is three-dimensional and it is worth asking whether a mapping function, given that the ionosphere is more accurately described in three dimensions, can ever be as simple as that of equation (19). The answer, unfortunately, is "no". A few simplistic geometry examples will prove this, followed by a more detailed analysis based on actual data.

[27] Geometry Example 1: Presume, for now, that the three-dimensional ionosphere is made up of a purely homogenous density distribution of electrons (N_e = constant). This can be visualized in Figure 1, with the presumption of a constant N_e value. Although this does not constitute a "condensed shell", one can still define some radius (r_s) as the place where the piercing angle (z') occurs. Since N_e is assumed constant, the relationship between s and STEC and that between d and VTEC are found in equation (12). Similarly, the relationship between STEC and VTEC is found in equation (13). However, since we no longer assume the ionosphere to be infinitesimally thin, the exact length of s is computed from equation (4). As such, the mapping function (W_{hs}, where the "hs" subscript is for "homogenous sphere") is exactly that of equation (18), without taking any limit, and where we replace the "nfs" subscript with "hs":

$$W_{hs} = \frac{s_{hs}}{d_{hs}} = \frac{1}{\cos(z')} + \frac{\cos^2(z') - 1}{8r_s^2 \cos^5(z')} d_{hs}^2 + \frac{7 - 10\cos^2(z') + 3\cos^4(z')}{128 r_s^4 \cos^9(z')} d_{hs}^4 + \ldots \quad (20)$$

To gain an appreciation for the magnitude of the second- and fourth-order terms of equation (20), some nominal values were chosen and their impacts quantified in Table 1. For the sake of this example, the bottom and top radii of the ionosphere were chosen as 50 and 1000 km above the Earth's mean radius (r_e) of 6371 km.

[28] What Table 1 basically says is that if the ionosphere is not modeled as a two-dimensional spherical shell, but is instead allowed to retain its three-dimensional (spherical) shape under the simple assumption of N_e = constant, that the use of $1/\cos(z')$ (the zeroth-order term) as a stand-in for the mapping function yields errors ranging from a few hundredths of a percent up to 15%, depending on choice of shell height and angle of ray piercing.

[29] Note also that in this model of the ionosphere, for the most part, the percent error between the W_{hs} value and that approximated by $1/\cos(z')$ is almost always positive, with the only exceptions being for shells over 400 km high or else for extreme z' values for shells at 400 km. This indicates that one can expect that using $1/\cos(z')$ will, on average, yield a systematically too large value of W_{hs}. Applying this conclusion to equation (11), it can be concluded that using the standard $1/\cos(z')$ mapping function to determine MSTEC from VTEC in a spherical shell model should, for the most part, yield MSTEC values that are systematically too large. (Replace "too small" with "too large" for shells at 500 km height.) Of course, this continues to rely on the overly simple N_e = constant assumption over the entire ionosphere.

[30] Finally, as a matter of explanation, there is no entry for $z' = 70°$ in Table 1 at 500 km because it is geometrically impossible for a ray (beginning at re =

Table 1. Magnitude of Terms, and Error Associated With Truncation, in the Mapping Function (W_{hs}) Assuming the Ionosphere Is Spherically Three-Dimensional (Between 50 and 1000 km Above the Earth's Surface) and of Constant Electron Density

Shell Height (km) (=$r_s - r_e$)	z'	Zeroth-Order Term	Second-Order Term	Fourth-Order Term	Percent Error Ignoring All Second- and Higher-Order Terms
200	10	1.015	-8.50×10^{-5}	4.83×10^{-7}	0.12%
200	30	1.155	-1.34×10^{-3}	1.48×10^{-5}	1.31%
200	50	1.556	−0.014	6.16×10^{-4}	4.80%
200	70	2.924	−0.493	0.313	15.12%
300	10	1.015	-8.25×10^{-5}	4.55×10^{-7}	0.09%
300	30	1.155	-1.30×10^{-3}	1.39×10^{-5}	0.86%
300	50	1.566	−0.014	5.80×10^{-4}	2.91%
300	70	2.924	−0.478	0.295	4.65%
400	10	1.015	-8.01×10^{-5}	4.29×10^{-7}	0.04%
400	30	1.155	-1.26×10^{-3}	1.31×10^{-5}	0.38%
400	50	1.556	−0.131	5.46×10^{-4}	0.94%
400	70	2.924	−0.464	0.278	−9.01%
500	10	1.015	-7.78×10^{-5}	4.04×10^{-7}	−0.00%
500	30	1.155	-1.23×10^{-3}	1.24×10^{-5}	−0.09%
500	50	1.556	−0.013	5.15×10^{-3}	−1.10%

6371 km) to pierce the 500 km high shell at an angle greater than 68.007°.

[31] Geometry Example 2: As in Geometry Example 1, allow the ionosphere to retain three dimensions, but consider that all of the electrons are contained in a limited, high density region (the "F region", as it is known) of constant electron density (N_e). Let that region not be a shell of zero thickness, but instead be limited to ± 50 km surrounding a central radius "r_s". This is a somewhat more realistic model, which accounts for a large majority of the actual distribution of electrons in the ionosphere. In a manner similar to Geometry Example 1, the terms and truncation error for the mapping function can be computed. However, because the ionosphere is limited to a tight 50 km band around the central radius, the error in slant length is reduced, as is the error in using $1/\cos(z')$ as the mapping function. The results are shown in Table 2.

[32] Note that while the size of the truncation error is reduced in this example, from that of example 1, it is always systematically negative. Since this example represents a large portion of the total electron density of the ionosphere, it may be appropriate to conclude that the use of $1/\cos(z')$ to map STEC from VTEC probably will yield systematically low values under any shell model of reasonable r_s.

[33] Obviously the real ionosphere is going to have electrons outside of this tight band of example 2, but not

Table 2. Magnitude of Terms, and Error Associated With Truncation, in the Mapping Function Assuming the Ionosphere Is Spherically Three-Dimensional (Within ± 50 km of Central Radius "r_s") and of Constant Electron Density

$r_s - r_e$ (km)	z'	Zeroth-Order Term	Second-Order Term	Fourth-Order Term	Percent Error Ignoring All Second- and Higher-Order Terms
200	10	1.015	-9.42×10^{-7}	5.93×10^{-11}	−0.000%
200	30	1.155	-1.49×10^{-5}	1.82×10^{-9}	−0.003%
200	50	1.556	-1.55×10^{-4}	7.56×10^{-8}	−0.020%
200	70	2.924	-5.46×10^{-3}	3.84×10^{-5}	−0.373%
300	10	1.015	-9.14×10^{-7}	5.58×10^{-11}	−0.000%
300	30	1.155	-1.44×10^{-5}	1.71×10^{-9}	−0.002%
300	50	1.566	-1.50×10^{-4}	7.12×10^{-8}	−0.019%
300	70	2.924	-5.30×10^{-3}	3.62×10^{-5}	−0.362%
400	10	1.015	-8.88×10^{-7}	5.26×10^{-11}	−0.000%
400	30	1.155	-1.40×10^{-5}	1.61×10^{-9}	−0.024%
400	50	1.556	-1.46×10^{-4}	6.71×10^{-8}	−0.019%
400	70	2.924	-5.14×10^{-3}	3.41×10^{-5}	−0.351%
500	10	1.015	-8.62×10^{-7}	4.96×10^{-11}	−0.000%
500	30	1.155	-1.36×10^{-5}	1.52×10^{-9}	−0.002%
500	50	1.556	-1.42×10^{-4}	6.33×10^{-8}	−0.341%

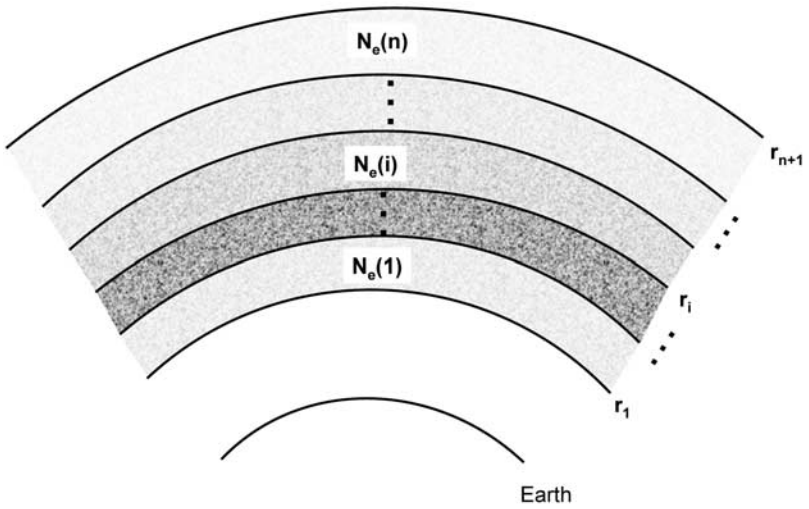

Figure 4. Geometry of an idealized ionosphere of individually constant, stratified layers.

quite as widely and homogenously spread as that of example 1. As such, the actual geometry-based error in using equation (8) will likely have a magnitude somewhere between those found in Tables 1 and 2. It is not possible to delve further into this geometric error without the introduction of more detailed information on the actual distribution of electrons in the ionosphere itself, so that will be the subject of the next section.

8. US-TEC Model

[34] The US-TEC model uses a set of empirical orthonormal functions (EOFs) to characterize the vertical variation in electron density through the ionosphere. These orthonormal functions are calculated at the start of each day using a singular-value decomposition algorithm based on the vertical density profiles from the IRI95 model. Exactly three EOFs are used in the US-TEC model. Increasing the number of EOFs beyond three achieves only negligible improvement in the accuracy. The state vector in the Kalman filter consists of a set of amplitude coefficients for these EOFs, which describes the vertical structure. The amplitude coefficients for each grid point, with a geographic spacing of 1.5° latitude and 4.0° longitude, are calculated every 15 min. The resultant model provides a succinct representation of the electron density field in four dimensions.

[35] The input data to US-TEC are 115 continuously operating, permanent GPS receivers distributed around the United States and Canada. Data are received by NOAA's Space Weather Prediction Center in real-time, and therefore allow very low latency computations. In US-TEC, the Kalman filter uses the IRI95 model to propagate the state and its associated covariance matrix to the next observation set, every 15 min. The forward propagation of the state is constructed from a weighted linear combination of the relative spatial/temporal gradients in IRI95 and an absolute estimate from IRI95. Correlations are assumed between neighboring grids in the latitude and longitude directions where the amount of correlation decreases with distance, on the basis of a Gaussian function. No covariance, and therefore no correlation, is assumed in the radial direction. Model errors are also included in the propagation of the state covariance. Details can be found in the work by *Spencer et al.* [2004].

9. Using US-TEC to Approximate the Expected Geometry-Based Mapping Error

[36] Although US-TEC is a model of the ionosphere, it is based on adjusting the plasma density profiles from the IRI empirical model [*Spencer et al.*, 2004; *Fuller-Rowell et al.*, 2006] based on ground-based, dual-frequency, GPS receiver observations. Validation of the output indicates an accuracy of less than 2 TEC units in the average slant content [*Araujo-Pradere et al.*, 2007; *Minter et al.*, 2007] making the data ideal for evaluating the validity of using a shell model. Because it has a full four dimensions of data (latitude, longitude and height, plus time), a great deal of analysis can be done using this data. One such analysis will be a more comprehensive look at how the spherical geometry impacts the error in using $1/\cos(z')$ to map STEC from VTEC. Before going on to a full data analysis, one final example to quantify the geometric error will be presented.

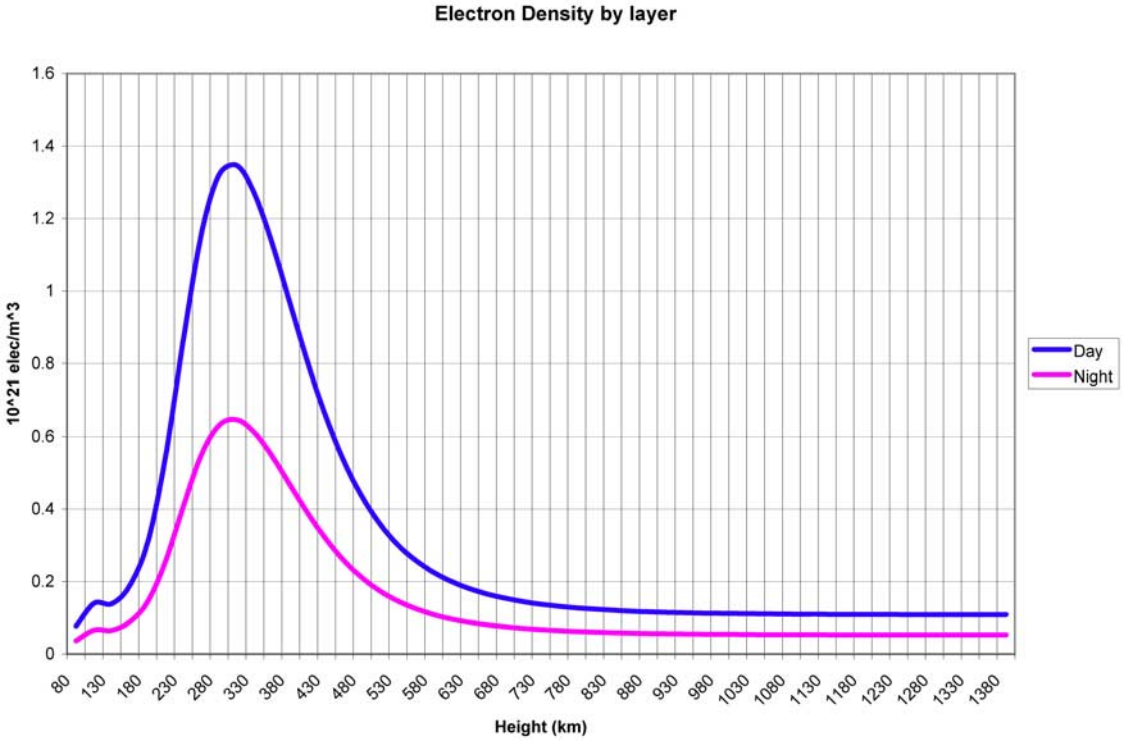

Figure 5. Average electron density of USTEC, by layer, for 12 May 2006.

[37] Geometry Example 3: Allow the ionosphere to retain three dimensions, and allow the density of electrons to be stratified into "n" discrete spherical layers, each one with a constant value of $N_e(i)$, $1 \leq i \leq n$ (see Figure 4). This is the most realistic, and frequently cited, approximation for the real distribution of the ionosphere without consideration of more complex vertical mixing. Although the ionosphere does not truly stratify in this way, on a calm ionospheric day it will tend toward some stratification [*Bilitza*, 2001].

[38] To find a "reasonable" stratification of the ionosphere, an average vertical profile was generated over the entire US-TEC area for a day of "average" (A_p = 16) ionosphere activity. The day used for this test was 12 May 2006. For that day, the average vertical profile of US-TEC was generated, and these N_e values assigned to the 53 distinct layers of US-TEC. Figure 5 shows the electron density of each of the 53 layers, with the two curves representing "day" and "night" hours. The heights of each of the 53 layers are given along the X axis, with the associated electron density of that layer height given along the Y axis.

[39] As can be seen, the largest share of electrons is concentrated in the 300–350 km height area. As such, it may be expected that limiting the geometric mapping error in that region (by using a "shell height" around 300–350 km) might help minimize the total error. However, it is important to note that while the contributions of the highest layers are small (relative to the region of maximum density) they nonetheless sum up to a significant portion of the total number of electrons a raypath will intersect. In addition, the curvature of layers far removed from the shell itself may cause a growing "geometric error", even as the density of electrons in those layers is decreasing.

[40] In order to assess whether the small N_e contributions of higher layers are overwhelmed by the increasingly large geometric mapping errors of said layers, a few simple tests were performed. Consider first that in the discretized case of a 53 layer US-TEC model of the ionosphere the STEC, VTEC and MSTEC can be written as follows:

$$VTEC = \sum_{i=1}^{53} N_e(i) \cdot d(i) = d \cdot \sum_{i=1}^{53} N_e(i) \qquad (21)$$

$$STEC = \sum_{i=1}^{53} N_e(i) \cdot s(i) \qquad (22)$$

$$MSTEC = \frac{VTEC}{\cos(z')} = \frac{l}{\cos(z')} \cdot \sum_{i=1}^{53} N_e(i) \cdot d(i)$$
$$= \sum_{i=1}^{53} N_e(i) \cdot s^M \quad (23)$$

In the above equations, $N_e(i)$ refers to the number of electrons in each of the 53 layers, while s(i) refers to the slant length along the raypath through each of the 53 layers. Each layer will have a unique s(i) value, computed by inserting the layers top and bottom radii into equation (4). The value z′ occurs by choosing some particular shell, $r = r_s$ by which the computing of MSTEC from VTEC will be done. (Note that US-TEC, being a three-dimensional model, has no inherent "shell" height though. For this paper, a variety of shell heights will be chosen for study.)

[41] The value of d(i), the vertical length through each of the 53 layers, has this constant value for US-TEC:

$$d(i) = 25km = d \quad (24)$$

Note the similarity between equations (22) and (23). In order to draw on their similarity, the variable "s^M" has been introduced in equation (23), and will be referred to as the "mapped slant length". This is not to be confused with the true slant length, s(i), which is found in equation (22). The equation for s^M can be deduced from equation (23) as:

$$s^M = \frac{d}{\cos(z')} \quad (25)$$

[42] The mapped slant length (s^M) for each layer "i" will thus be constant, since d is constant (25 km), and the piercing angle is a constant for any given ray and shell choice. In equations (22) and (23) the only difference is the use of s(i) in (22) (for STEC) and s^M in (23) (for MSTEC). It is exactly for this reason that the "geometric error" grows larger as one investigates layers further and further away from the $r = r_s$ shell, since s^M, remains constant and increasingly fails to accurately approximate the true slant length at a layer, s(i). The layers farthest from a chosen "r_s" shell will have the largest difference between s(i) and s^M. However, as most reasonable "r_s" values will lie near the area of densest N_e values it is also true that those remote layers will have less N_e to contribute to the overall STEC anyway. The real question then is whether the geometric errors of layers far from r_s will be outweighed by the smallness of their N_e contributions.

[43] In this idealized and discretized case where the geometry and stratification of the model are known, it is possible to actually sum up the STEC and VTEC values as implied by the USTEC model. In addition, one may choose any r_s shell and use that to compute z′ and thus MSTEC. With this in mind, the total (geometry-only) error ("E") of using a shell and simple $1/\cos(z')$ mapping function to approximate STEC by MSTEC is computed as:

$$E = STEC - MSTEC = \sum_{i=1}^{53} N_e(i) \cdot s(i) - \sum_{i=1}^{53} N_e(i) \cdot s^M$$
$$= \sum_{i=1}^{53} N_e(i) \cdot \left[s(i) - s^M\right] = \sum_{i=1}^{53} N_e(i) \cdot \left[s(i) - \frac{25km}{\cos(z')}\right] \quad (26)$$

where the individual contribution of each layer to the total error will be represented as:

$$\varepsilon(i) = N_e(i) \cdot \left[s(i) - s^M\right] \quad (27)$$

Equation (27) helps exemplify what was mentioned before: For each layer further and further from the shell (especially higher), $N_e(i)$ grows smaller, but $[s(i) - s^M]$ grows larger and the question of interest is whether the combined quantity, $\varepsilon(i)$ shrinks or grows as the one moves into "i" layers high above the shell.

[44] In order to quantify the size of errors in equation (26), and how each layer contributes to them, a sampling of shell heights and piercing angles were tested. Table 3 shows the total errors incurred in this example:

[45] These data are presented graphically in Figure 6. Notice in that figure that the signature of these errors is not highly complex, and definitely able to be modeled by a simple function (quadratic, logarithmic or other). However, the coefficients of such a function would depend upon time of day, shell height, piercing angle and of course absolute knowledge of the stratification of the ionosphere.

Table 3. Total Error (= E = STEC-MSTEC) Incurred in Using $1/\cos(z')$ Mapping Angle in a 53 Layer Perfectly Stratified "Average" Spherical Ionosphere[a]

Shell Height (km)	Piercing Angle at Shell Height (z′) (deg)						
	5	15	25	35	45	55	65
200 (day)	∼0	−0.012	−0.039	−0.094	−0.212	−0.489	−1.256
200 (night)	∼0	−0.006	−0.019	−0.045	−0.103	−0.237	−0.608
300 (day)	∼0	−0.008	−0.025	−0.060	−0.134	−0.304	−0.753
300 (night)	∼0	−0.004	−0.012	−0.029	−0.065	−0.148	−0.367
400 (day)	∼0	−0.003	−0.010	−0.024	−0.051	−0.100	−0.132
400 (night)	∼0	−0.002	−0.005	−0.012	−0.025	−0.050	−0.070
500 (day)	∼0	0.001	0.004	0.012	0.037	0.127	0.664
500 (night)	∼0	0.001	0.002	0.006	0.017	0.059	0.312

[a]Units are TECU.

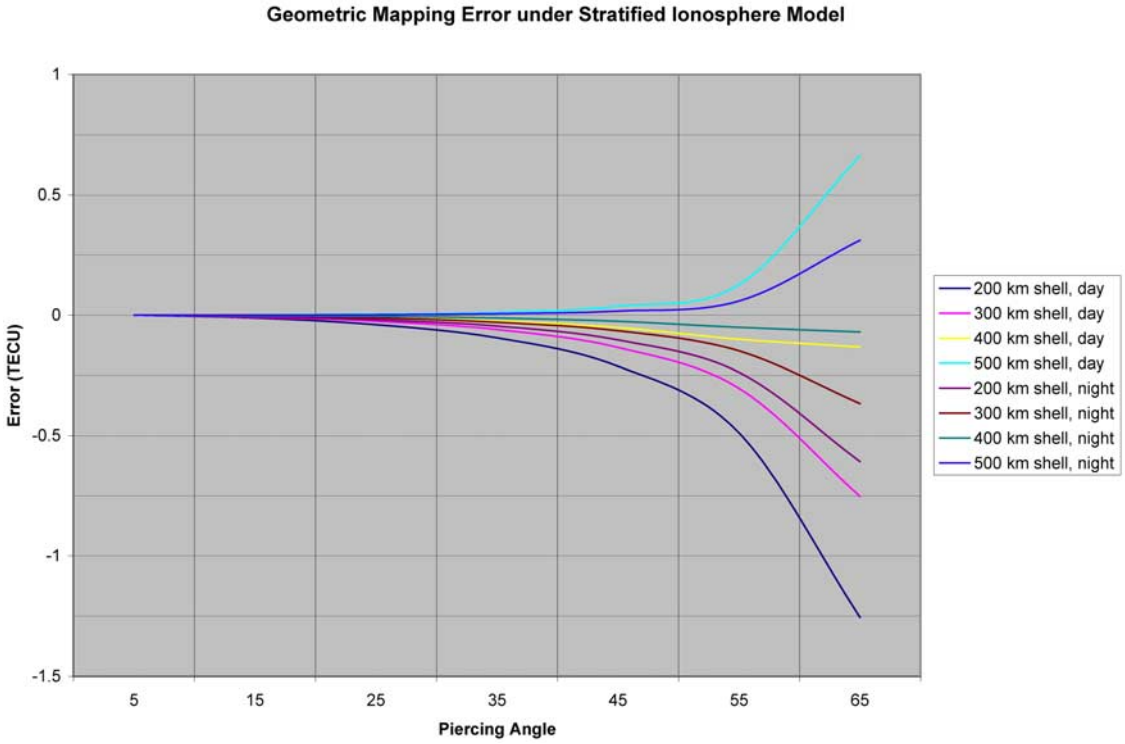

Figure 6. Total error (MSTEC – STEC) induced in an idealized 53 layer stratified ionosphere by using a simple cosine mapping angle and a variety of spherical shell heights.

[46] However, if one looks at the ratio of E to STEC (shown in Table 4) it is seen that the time-of-day dependence is effectively removed (leaving dependence on shell height, piercing angle and layer stratification only). This indicates that, if the actual stratification of the ionosphere were to follow the one chosen on this particular day, that a simple scale factor can be applied (based on shell height and piercing angle) which will alleviate the effect of the systematic geometric error, E.

[47] Table 4 is represented graphically in Figure 7, where a few things can be seen. First off, looking at one shell at a time, one can see an asymptotic behavior (which turns out to be nicely estimated by an arctangent, as will be seen next) as the piercing angle goes from 65 to 0 degrees. However, looking at one piercing angle at a time, it is clear that there is a linear trend to the percent error as the shell height changes from 200 km high to 500 km high. These simple observations will be used to propose a modification to the "original" mapping function (equation (8)) later.

[48] Prior to proposing a modification to the mapping function, let us turn our attention to the question of layer-by-layer contributions to the geometric error. Breaking down the total error (E) into its layer-by-layer contributions ($\varepsilon(i)$), one can begin to answer whether the shrinking $N_e(i)$ or growing $[s(i) - s^M]$ values dominate higher layers. Figures 8–11 show the contribution of each layer to the total geometry error. In order to arrive at the total error (as shown in Table 3), the integral under each curve in Figures 8–11 must be performed (normalized against the distance between the top and bottom layers.) There are a few interesting things to note in those figures. First, the transition from those layers yielding a positive error to those yielding negative error occurs (predictably) at the layer height corresponding to the

Table 4. Ratio of Total Error (E) Relative to STEC[a]

Shell Height (km)	Piercing Angle at Shell Height (z') (deg)						
	5	15	25	35	45	55	65
200 (day)	−0.03	−0.28	−0.84	−1.86	−3.68	−7.10	−14.36
200 (night)	−0.03	−0.28	−0.85	−1.88	−3.71	−7.15	−14.47
300 (day)	−0.02	−0.18	−0.54	−1.18	−2.30	−4.30	−8.14
300 (night)	−0.02	−0.18	−0.54	−1.19	−2.32	−4.36	−8.26
400 (day)	−0.01	−0.08	−0.22	−0.48	−0.87	−1.38	−1.34
400 (night)	−0.01	−0.08	−0.23	−0.49	−0.89	−1.44	−1.47
500 (day)	+0.00	+0.03	+0.09	+0.24	+0.61	+1.69	+6.22
500 (night)	+0.00	+0.03	+0.09	+0.23	+0.58	+1.63	+6.08

[a]Units are percent.

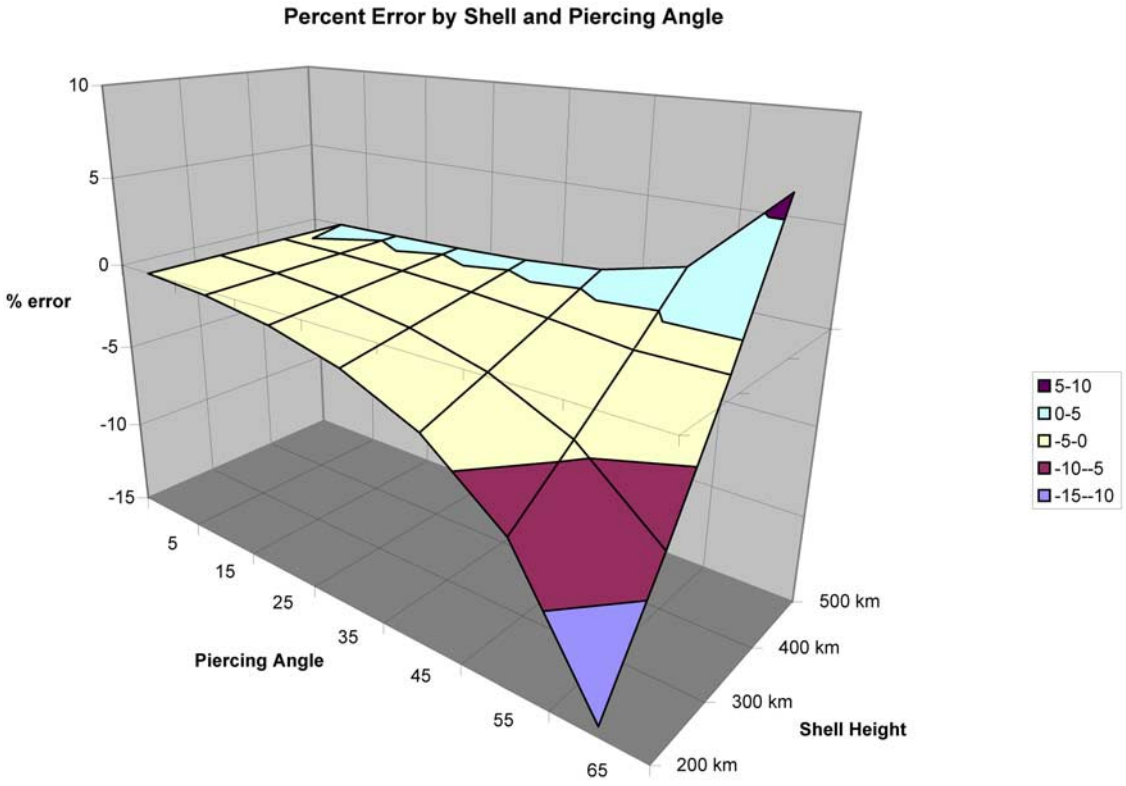

Figure 7. Percentage error ((STEC – MSTEC)/STEC)*100% induced in an idealized 53 layer stratified ionosphere by using a simple cosine mapping angle and a variety of spherical shell heights.

chosen shell. This is due to the fact that geometry errors go to zero [$s(i) = s^M$] at the shell. Secondly, it can be seen that the greater piercing angles tend to generate larger bulges of error in approaching the shell, as well as thicker ''tails'' for layers above the shell. However, despite the size of the preshell bulge, or the postshell tail, the real story is that each layer does contribute to the geometric error and unless the positive and negative aspects just happen to be perfectly balanced, the fact is that geometry alone will yield a nonzero systematic error in MSTEC.

[49] One final and cautionary note is that the tails of all functions seen in Figures 8–11 do not asymptotically approach zero at the maximum height of US-TEC. This implies that the density of electrons is not shrinking fast enough to overwhelm the growing geometry error as the layers get farther and farther from the shell. Eventually, of course, the number of electrons will approach zero and the geometric errors will be of no consequence. But at least at the 1400 km height (top of US-TEC), there appears to be still significant electron density which should yield even more systematic error if the ''tails'' in Figures 8–11 were allowed to extend to the top of the ionosphere (wherever that might lie).

[50] As predicted in ''Geometric Example 2'', the actual percentage error incurred by using a simple $1/\cos(z')$ mapping function (shown in Table 4) has a purely geometric signal which falls between a few hundredths of a percent to as large as 14%. Also, the sign of this systematic (purely geometric) error is constant for a chosen shell height. As such, this third example proves that even if the ionosphere is treated as a known series of stratified layers, that the use of $1/\cos(z')$ will always yield an MSTEC value which is systematically too large or too small, relative to STEC (depending on chosen shell height).

10. Modified Mapping Function

[51] In the three geometric examples provided, it has been shown that there will always be a systematic component to the error induced by reliance upon $1/\cos(z')$

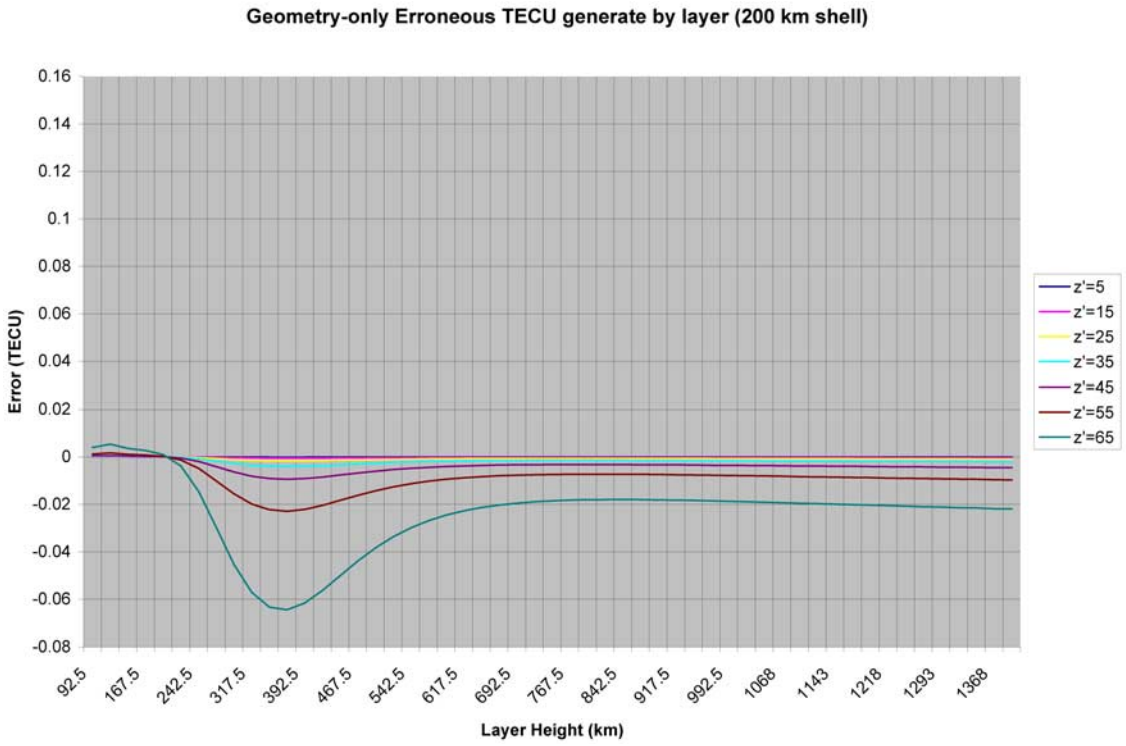

Figure 8. Layer-by-layer contribution to the total geometry error for a perfectly stratified ionosphere if a 200 km shell is chosen for mapping VTEC into STEC.

as the sole mapping function for MSTEC. But it has also been shown that this systematic error is dependent both upon the actual distribution of electrons and how that distribution relates to the choice of shell height. Can a better, generic mapping function be proposed which attempts to model and remove this systematic error? Possibly, but only under certain presumptions: (1) The precondensed ionosphere is stratified and (2) that stratification is known. These conditions are quite limiting due to the fact that the electron density depends on time of day, and that any vertical structure will make such an attempt fruitless. Is the average stratification of 12 May 2006 a good estimate of the ionosphere? Maybe, but attempting to find a better mapping function between VTEC and STEC seems somewhat futile when the distribution of the ionosphere changes in space and time in ways that are too difficult to rely on a shell model anyway.

[52] On the other hand, it should be pointed out that shell models (despite known problems) will probably continue to be popular methods for modeling the ionosphere into the future. As such, a simple "fix" to the basic $1/\cos(z')$ version of $\hat{W}$ will be proposed, based on the data of Table 4 and the graphical observation of that data in Figure 7.

[53] First, recall that Table 4 has "percent error" (which will be given the variable "p"):

$$p = \frac{STEC - MSTEC}{STEC} \times 100\% \tag{28}$$

where MSTEC = (VTEC/cos(z′)).

[54] Recall that the entire goal of the mapping function is to estimate STEC from VTEC and "shell information" (piercing angle, for example). As such, solving equation (28) for STEC and expanding the original "MSTEC" function, we arrive at:

$$\begin{aligned} STEC &= \frac{1}{1-(p/100)} \times MSTEC \\ &= \frac{1}{1-(p/100)} \times \frac{VTEC}{\cos(z')} \\ &= \frac{VTEC}{(1-(p/100)) \times \cos(z')} \end{aligned} \tag{29}$$

Thus, the proposed new mapping function takes this form:

$$\hat{W}_{new} = \frac{1}{(1-(p/100)) \times \cos(z')} \tag{30}$$

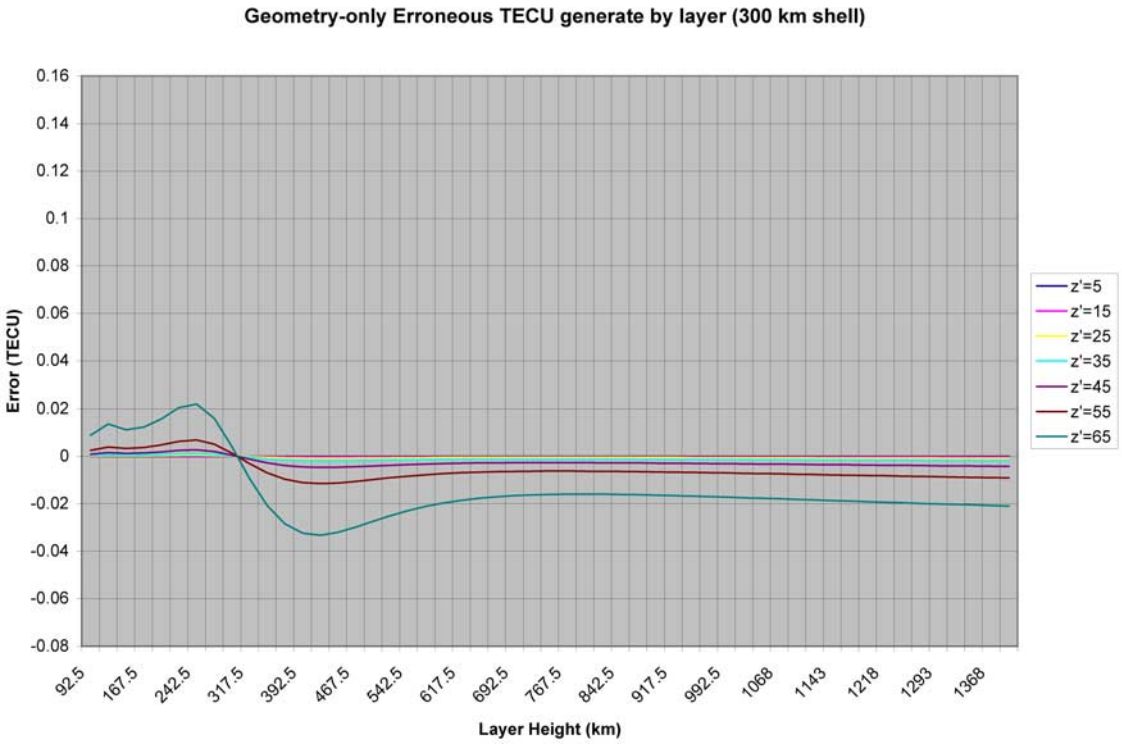

Figure 9. Layer-by-layer contribution to the total geometry error for a perfectly stratified ionosphere if a 300 km shell is chosen for mapping VTEC into STEC.

[55] The values for p depend on z' and r_s. Either a lookup table could be used or else (for simplicity of coding) a generic functional representation of p can be sought. That is where the observations of Figure 7 were useful. In order to fit a function to the data of Table 4, each z' value was allowed to have a linear fit for p across all r_s (or h) values, and then the coefficients of those lines ("a" and "b") were fit to arctangents, as such:

$$\begin{aligned} p &= a + b \cdot h \\ a &= (-\arctan[(z' - a_0) \cdot a_1] - a_2) \cdot a_3 \\ b &= (-\arctan[(z' - b_0) \cdot b_1] - b_2) \cdot b_3 \end{aligned} \tag{31}$$

where z' is given in degrees, h is the shell height in kilometers (equal to r_s minus the mean Earth radius), and the following coefficients fit the data of Table 4 best in a least squares sense:

$$\begin{aligned} a_0 &= 64.4297 & b_0 &= 64.3659 \\ a_1 &= 0.0942437 & b_1 &= 0.104974 \\ a_2 &= 1.39436 & b_2 &= 1.41152 \\ a_3 &= 19.6357 & b_3 &= -0.0463341 \end{aligned}$$

[56] This new mapping function obviously is predisposed to agree better with the stratified ionosphere model, since it was derived directly from it. As such, it will be unnecessary to test it against that model. However, this mapping function will be examined for its usefulness in later sections, against actual 3-D vertically mixed data to see if it adds any accuracy.

[57] All of the above examples have only examined the geometric problems arising from reliance upon $1/\cos(z')$ as the mapping function between VTEC and MSTEC. In the following sections, the problem of the ionosphere having a complex distribution (far from being simply stratified) will be examined, and its impact on MSTEC vs STEC quantified. As will be shown, this error is the real error of using a shell model, as it will be shown to dominate the total error budget, making these geometric errors seem small by comparison.

11. Quantifying Overall STEC Errors Using US-TEC

[58] The previous sections have dealt with idealized electron distributions in an attempt to simplify the quantification of errors associated with the use of a shell

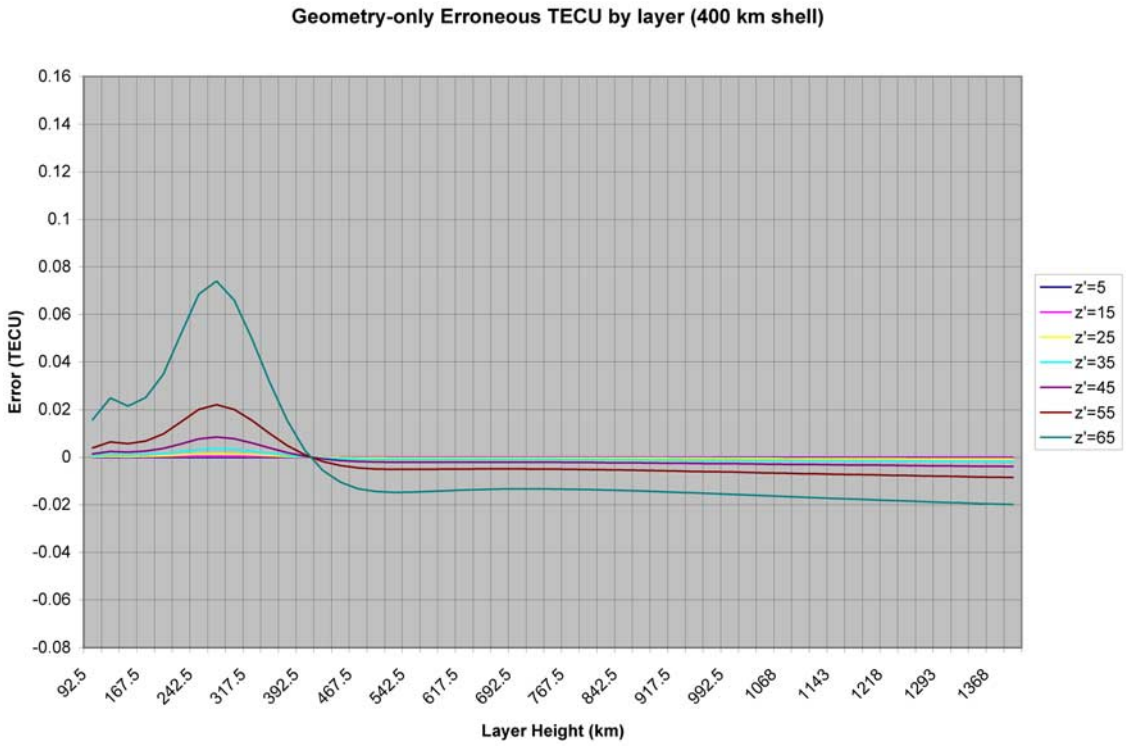

Figure 10. Layer-by-layer contribution to the total geometry error for a perfectly stratified ionosphere if a 400 km shell is chosen for mapping VTEC into STEC.

model. Obviously such simplifications are limited in what they can contribute to the overall understanding of the errors. In order to further expand this study, it is necessary to take a reliable, realistic 3-D (vertically mixed) model of the ionosphere and compute the actual STEC seen through such a model and compare it with the MSTEC which would be computed if the 3-D model were replaced with a 2-D shell model and some mapping function.

[59] Few such models exist. However, one readily available, and reliable model is the previously mentioned US-TEC [*Spencer et al.*, 2004], of the Space Weather Prediction Center (SWPC) of the National Oceanic and Atmospheric Administration (NOAA's) National Weather Service (NWS). This model covers the region from 10 to 60 degrees north latitude (by 1.5 degree increments), 220 to 300 degrees east longitude (by 4.0 degree increments), and from 80 to 1400 km above an average Earth radius (by 25 km increments).

[60] A grid of points, spaced across the conterminous United States was used as the points of interest. At each of these points, the actual STEC value along a raypath from the grid point to each visible GPS satellite was integrated through the three-dimensional US-TEC ionosphere model. (In fact, SWPC provides these integrated values as a series of grids, precomputed.) While these values come from US-TEC, which is a model of the ionosphere, they are the true integration along raypaths from the grid points of interest, through US-TEC. As such, these STEC values will be, for the purposes of this paper, considered "control" STEC values, against which the MSTEC values will be compared. The VTEC values for the shell models were created by integrating the US-TEC model vertically at each latitude and longitude combination in the 3-D grid in order to get an electrons/square-meter value to place at a grid location on any given shell. Since any given shell model uses its own specific shell height, these vertically integrated values were applied to a variety of popular shell heights (200 km to 500 km) in order to generate a family of shell models for testing.

[61] Using the US-TEC data, and the family of derivative shell models therefrom, a set of data was examined spanning 12 April 2006 to 12 September 2006. Two mapping functions were used to generate MSTEC: the original ($1/\cos(z')$), and the new $\hat{W}_{new}$ from equation (30). Statistics of E (the difference between STEC and MSTEC) were generated using these two different mapping functions. These E data were parsed into a variety of categories, including Satellite Vehicle Number, Latitude,

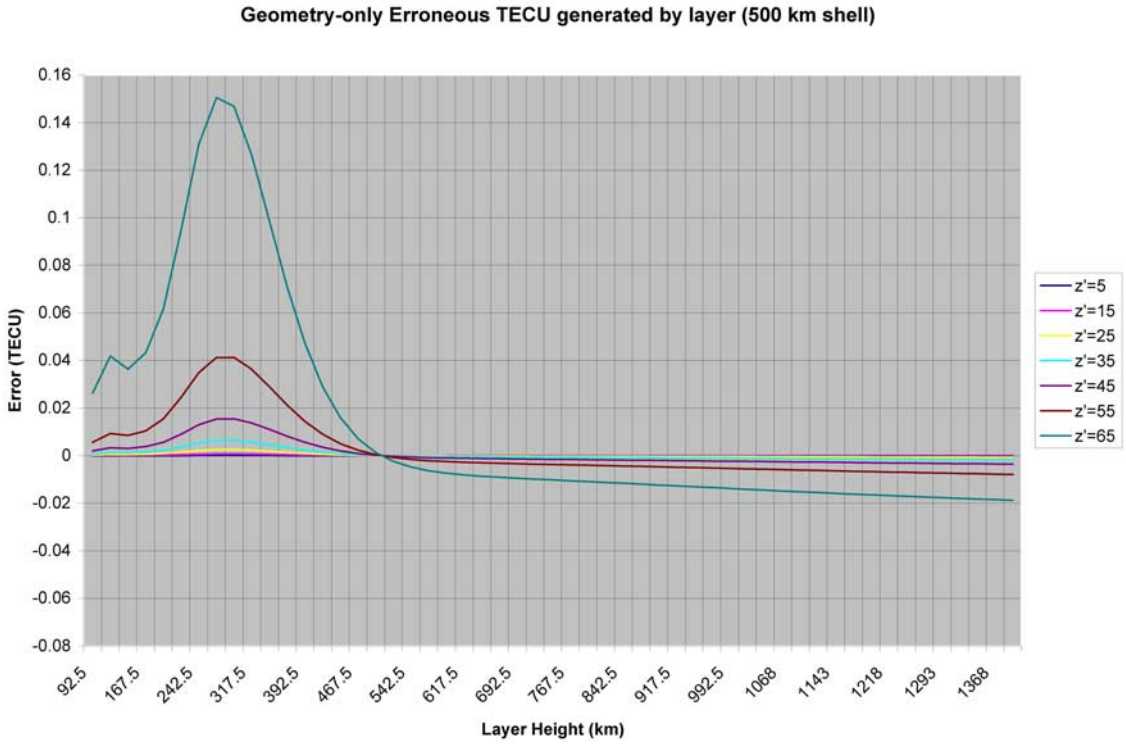

Figure 11. Layer-by-layer contribution to the total geometry error for a perfectly stratified ionosphere if a 500 km shell is chosen for mapping VTEC into STEC.

Longitude, Shell Height, Angle above the Horizon, Time of Day, and the ionosphere activity index "A_p". The initial statistics showed no significant statistical correlation with Longitude nor with Satellite Vehicle number, so further analysis using these two variables was not pursued. However, the other five variables definitely had a quantifiable impact in the E values and are presented next. Before looking at interactions between parameters, the basic statistical data for each variable independently are presented in Tables 5–9.

[62] It should be noted that Tables 5–9 all represent the same data, but grouped for a different independent variable on each table. The purpose of these five different tables is to answer two main questions of this paper: (1) Does the new mapping function show an improvement over the old mapping function? (2) How well or how poorly do shell models behave with respect to a particular variable (time of day, etc.)? Further discussion of these two questions is provided for each table.

Table 5. STEC – MSTEC by Latitude[a]

North Latitude	Number of Values	Average	Standard Deviation	RMS	Minimum	Maximum
10–20	664×10^6	−1.4	4.3	4.5	−97.7	+43.9
		−0.2	**2.1**	**2.1**	**−64.2**	**+44.3**
20–30	801×10^6	−1.0	3.1	3.3	−74.1	+30.4
		−0.0	**1.8**	**1.8**	**−40.2**	**+35.7**
30–40	824×10^6	−0.8	2.6	2.7	−67.2	+30.8
		+0.0	**1.5**	**1.5**	**−44.0**	**+38.5**
40–50	802×10^6	−0.4	1.9	2.0	−41.4	+29.0
		+0.2	**1.1**	**1.1**	**−28.1**	**+32.6**
50–60	739×10^6	−0.3	1.4	1.4	−40.4	+35.5
		+0.2	**0.9**	**0.9**	**−28.1**	**+38.5**

[a]Units are TECU. All shells, all times, all horizon angles, all A_p values. Statistics using the original $1/\cos(z')$ function are shown in nonbold type. Statistics using the new mapping function ($\hat{W}_{new}$) are shown in bold type.

Table 6. STEC – MSTEC by Time of Day[a]

Hour of Day (UTC)	Number of Values	Average	Standard Deviation	RMS	Minimum	Maximum
0–2	313×10^6	−1.1	3.5	3.7	−74.5	+33.8
		+0.0	**1.8**	**1.8**	**−46.5**	**+37.0**
2–4	*309×10^6*	*−0.8*	*2.7*	*2.8*	*−69.5*	*+35.5*
		+0.0	***1.4***	***1.4***	***−43.6***	***+38.5***
4–6	*303×10^6*	*−0.6*	*1.9*	*2.0*	*−48.3*	*+20.7*
		+0.0	***1.1***	***1.1***	***−29.2***	***+31.7***
6–8	*299×10^6*	*−0.4*	*1.5*	*1.5*	*−33.2*	*+23.1*
		+0.0	***0.9***	***0.9***	***−22.6***	***+23.1***
8–10	*305×10^6*	*−0.3*	*1.2*	*1.3*	*−28.7*	*+10.4*
		+0.0	***0.7***	***0.7***	***−17.8***	***+12.9***
10–12	*314×10^6*	*−0.4*	*1.4*	*1.4*	*−24.5*	*+9.8*
		+0.0	***0.8***	***0.8***	***−17.5***	***+13.2***
12–14	*328×10^6*	*−0.5*	*1.8*	*1.9*	*−37.6*	*+13.0*
		+0.0	***1.0***	***1.0***	***−26.9***	***+15.5***
14–16	337×10^6	−0.7	2.4	2.6	−58.3	+18.1
		+0.1	**1.3**	**1.3**	**−34.2**	**+25.2**
16–18	342×10^6	−0.9	3.1	3.2	−87.0	+24.8
		+0.1	**1.6**	**1.6**	**−56.1**	**+28.1**
18–20	336×10^6	−1.1	3.7	3.8	−84.2	+25.6
		+0.1	**2.1**	**2.1**	**−49.8**	**+30.8**
20–22	328×10^6	−1.1	4.0	4.2	−97.7	+43.9
		+0.2	**2.3**	**2.3**	**−64.2**	**+44.3**
22–24	316×10^6	−1.2	4.0	4.2	−85.7	+30.8
		+0.1	**2.1**	**2.1**	**−51.4**	**+30.5**

[a]Units are TECU. All shells, all horizon angles, all latitudes, all A_p values. Areas in italics indicate "night" in the Central Time Zone. Statistics using the original $1/\cos(z')$ function are shown in nonbold type. Statistics using the new mapping function ($\hat{W}_{new}$) are shown in bold type.

[63] A few things are clear from this table. The first is that points in the midlatitudes have more data. This is simply because such points fall under the central area of US-TEC and therefore have more receiver-satellite raypaths which pass through the complete US-TEC grid. Also, note that the statistics of E definitely improve as one moves away from the equator northward. Although such impacts could be explained from a variety of sources, the most likely seems (to the authors) to be that ionosphere structure is greater, that is steeper gradients exist, in the southern part of CONUS than in the northern part. The southern United States is closer to the equatorial ionization anomaly (EIA), which is know to have more structure than at midlatitudes, and the northern part of the United States is still sufficiently far removed from the processes associated with auroral oval. Since greater ionosphere activity is expected to contribute to the inability of a shell model to properly reflect the true slant delays, it is reasonable to hypothesize that this south-to-north reduction in structure correlates to a south-to-north improvement in the agreement between USTEC-derived "control" slant delays and mapped slant delays.

[64] Additionally, while all of the above conclusions can be drawn for both the original or the new mapping functions, it is clear that using the new mapping function has reduced the bias (average E) significantly, as well as the overall agreement. (Standard deviations improved by 36% to 51%, depending on latitude.)

[65] Table 6 shows, by 2 hour time blocks, how E changes through out a day. Although the US-TEC model covers 4 time zones, the statistics can still be viewed as "day" and "night" by allowing the central time zone of the United States to approximate the US-TEC time for the general purposes of dividing the day into daytime and nighttime. Certain expected outcomes can be seen in Table 6, such as no strong correlation between the number of data points and time of day (as GPS satellites are visible day and night; note, however, that there is a moderate dropoff, indicating a slight increase in visible GPS satellites over the United States during the day). Also, as expected, the smaller ionospheric TEC values during the night yields better statistics for E. In fact, the strongest conclusion one could draw from this table would be "in absolute terms, using a shell model during the night is two to three times more reliable than using one during the day".

[66] As in Table 5, a comparison between the old and new mapping function statistics shows that the new mapping function generally removes all biases (average E tends toward 0.0) and the standard deviations improve by 30% to 50% as well, with the greatest improvement being the reduction of standard deviations during daylight hours.

Table 7. STEC – MSTEC by Angle Above the Horizon[a]

Horizon Angle	Number of Values	Average	Standard Deviation	RMS	Minimum	Maximum
0–5	292×10^6	−2.2	6.0	6.4	−94.6	+43.9
		+0.1	**3.0**	**3.0**	**−61.4**	**+44.4**
5–10	306×10^6	−1.9	5.1	5.5	−97.7	+33.8
		+0.1	**2.6**	**2.6**	**−64.2**	**+37.0**
10–15	311×10^6	−1.6	3.9	4.2	−85.3	+33.0
		+0.1	**2.1**	**2.1**	**−56.7**	**+36.7**
15–20	309×10^6	−1.2	2.8	3.1	−61.7	+29.0
		+0.2	**1.7**	**1.7**	**−38.4**	**+35.7**
20–25	301×10^6	−0.9	2.1	2.2	−45.0	+26.2
		+0.2	**1.4**	**1.4**	**−29.4**	**+27.6**
25–30	292×10^6	−0.6	1.6	1.7	−36.7	+18.8
		+0.1	**1.2**	**1.2**	**−26.2**	**+24.0**
30–35	284×10^6	−0.5	1.3	1.4	−32.1	+19.4
		+0.0	**1.0**	**1.0**	**−25.2**	**+20.1**
35–40	273×10^6	−0.4	1.1	1.1	−25.1	+17.0
		+0.0	**0.9**	**0.9**	**−20.7**	**+18.7**
40–45	256×10^6	−0.2	0.8	0.9	−20.9	+18.3
		−0.0	**0.7**	**0.7**	**−18.2**	**+18.8**
45–50	236×10^6	−0.2	0.7	0.7	−16.9	+14.3
		−0.0	**0.6**	**0.6**	**−15.0**	**+14.7**
50–55	213×10^6	−0.1	0.5	0.5	−13.9	+10.4
		−0.0	**0.5**	**0.5**	**−12.9**	**+11.3**
55–60	188×10^6	−0.09	0.4	0.4	−12.3	+8.3
		−0.01	**0.4**	**0.4**	**−11.3**	**+8.4**
60–65	164×10^6	−0.06	0.3	0.3	−11.8	+9.1
		−0.01	**0.3**	**0.3**	**−11.6**	**+9.2**
65–70	138×10^6	−0.04	0.3	0.3	−7.5	+7.8
		−0.01	**0.3**	**0.3**	**−7.1**	**+7.9**
70–75	111×10^6	−0.03	0.2	0.2	−5.3	+8.3
		−0.005	**0.2**	**0.2**	**−5.2**	**+8.3**
75–80	83×10^6	−0.01	0.2	0.2	−5.5	+5.0
		−0.002	**0.2**	**0.2**	**−5.5**	**+5.0**
80–85	53×10^6	−0.004	0.1	0.1	−3.9x	+3.4
		+0.000	**0.1**	**0.1**	**0.1**	**+3.4**
85–90	18×10^6	−0.002	0.2	0.2	−3.4	+3.7
		−0.003	**0.2**	**0.2**	**−3.4**	**+3.6**

[a]Units are TECU. All shells, all times, all latitudes, all A_p values. Statistics using the original $1/\cos(z')$ function are shown in nonbold type. Statistics using the new mapping function ($\hat{W}_{new}$) are shown in bold type.

[67] Table 7 breaks down the E statistics by elevation angle of the satellite above the horizon. Because it has been shown that the original mapping function, $1/\cos(z')$ gets progressively worse at low elevation angles, it is not at all a surprise to see the E statistics (based on the original mapping function) improve (in both average and standard deviation about the average) as raypaths move from near-horizon (0 to 5 degrees) to near-vertical (85–90 degrees). For the new mapping function, the improvement in standard deviation still occurs when going from near-horizon to near-vertical, but note that a significant portion of the bias (average E) has been removed by using the new mapping function, even at the lowest elevation angles.

[68] Although outliers continue to exist for near-vertical raypaths at the level of a few TECUs for both mapping functions, the overall statistics are quite good for these points. Still, the RMS of E exceeds 1.0 TECU at 40 degrees for the original mapping function (35 degrees for the new mapping function). If the need for TEC accuracy is at the 1.0 TECU level, then blindly applying a generic shell model (even with the new mapping function) simply will not suffice for satellites under 35 degrees above the horizon. And as can be calculated from the data counts, 62% of all raypaths occur below 35 degrees of elevation angle. That is a lot of data to ignore in order to gain 1.0 TECU accuracy from a shell model.

[69] Some very interesting information can be inferred from Table 7. First, and of critical importance, it must be remembered that US-TEC is built without any concept of a 2-D shell whatsoever. There is therefore no predisposition to any particular "shell height", though it should be mentioned that the underlying IRI95 model certainly does allow for regions of high density and low density. With this in mind, it is striking how clearly one can see

Table 8. STEC – MSTEC by Shell Height[a]

Shell Height (km)	Number of Values	Average	Standard Deviation	RMS	Minimum	Maximum
200	558×10^6	−2.9	4.9	5.7	−97.7	+40.6
		−0.3	**2.6**	**2.6**	**−64.2**	**+43.9**
250	555×10^6	−1.9	3.3	3.8	−70.0	+41.1
		−0.0	**1.9**	**1.9**	**−47.5**	**+44.1**
300	551×10^6	−1.2	2.1	2.4	−47.3	+42.3
		+0.1	**1.4**	**1.4**	**−33.9**	**+44.1**
350	547×10^6	−0.5	1.2	1.3	−33.7	+43.3
		+0.1	**1.0**	**1.1**	**−27.5**	**+44.3**
400	544×10^6	−0.01	0.9	0.9	−26.7	+43.9
		+0.17	**0.9**	**0.9**	**−26.1**	**+44.2**
450	539×10^6	+0.4	1.1	1.2	−24.8	+43.7
		+0.2	**0.9**	**0.9**	**−27.4**	**+43.4**
500	535×10^6	+0.8	1.6	1.8	−24.2	+42.6
		+0.2	**1.1**	**1.1**	**−28.1**	**+41.7**

[a]Units are TECU. All horizon angles, all times, all latitudes, all A_p values. Statistics using the original $1/\cos(z')$ function are shown in nonbold type. Statistics using the new mapping function ($\hat{W}_{new}$) are shown in bold type.

improvements in E by using a shell located at 400 km, as opposed to any other of the tested shells. The near zero average and sub-TECU standard deviation (for the original mapping function) indicate that, day or night, high satellite or low, at any latitude, one can, on average, get about 1 TECU of accuracy by using a 400 km shell. Remember that Table 7 indicated a cutoff angle of 35 degrees was required to yield sub-TECU accuracy. Clearly that result was based on all the bad statistics coming from the shells not located at 400 km altitude.

[70] It is also striking to notice that the new mapping function yields significant improvement to all shell models except that at 400 km (where, as we will see later, it has some positive and some negative impact over using the original mapping function). The fact that all shells except 400 km have a dramatic improvement in using the new mapping function can be inferred from Figure 7 where the percentage errors for all shells except 400 km have a nonzero signature.

[71] However, one slight disadvantage of 400 km shells, relative to lower shells is that as one uses a higher and higher shell, more rays can be drawn from receivers on the ground to the GPS SV's without intersecting the shell within its latitude and longitude range. Thus, as seen in Table 8, as shell height increases from 200 to 500 km, the number of actual values available for comparison is reduced from 558 million to 535 million. However, this slight disadvantage seems unimportant

Table 9. STEC – MSTEC by A_p Index[a]

A_p Index	Number of Values	Average	Standard Deviation	RMS	Minimum	Maximum
0–10	2677×10^6	−0.8	2.8	2.9	−85.7	+43.9
		+0.1	**1.5**	**1.5**	**−49.7**	**+44.3**
10–20	796×10^6	−0.8	2.9	3.0	−84.2	+29.4
		+0.1	**1.6**	**1.6**	**−51.4**	**+32.0**
20–30	267×10^6	−0.8	2.9	3.0	−97.7	+35.5
		+0.0	**1.6**	**1.6**	**−64.2**	**+38.5**
30–40	59×10^6	−0.7	3.0	3.1	−87.0	+25.2
		+0.0	**1.7**	**1.7**	**−56.1**	**+28.6**
40–50	0[b]	—	—	—	—	—
50–60	30×10^6	−0.5	2.2	2.3	−62.1	+22.7
		+0.1	**1.4**	**1.4**	**−31.8**	**+25.5**
60–70	0[b]	—	—	—	—	—
70–80	0[b]	—	—	—	—	—
80–90	0[b]	—	—	—	—	—
90–100	0[b]	—	—	—	—	—
100–110	0[b]	—	—	—	—	—
110–120	0[b]	—	—	—	—	—

[a]Units are TECU. All shells, all times, all latitudes, all horizon angles. Statistics using the original $1/\cos(z')$ function are shown in nonbold type. Statistics using the new mapping function ($\hat{W}_{new}$) are shown in bold type.

[b]No days with an A_p value in this range occurred during the study period.

Table 10. STEC – MSTEC by A_p Index[a]

A_p Index	Number of Values	Average	Standard Deviation	RMS	Minimum	Maximum
0–10	380×10^6	−0.0	0.85	0.85	−23.2	+43.9
		+0.2	**0.85**	**0.86**	**−22.7**	**+44.2**
10–20	113×10^6	−0.0	0.9	0.9	−24.0	+21.6
		+0.2	**0.9**	**0.9**	**−24.0**	**+22.2**
20–30	38×10^6	−0.0	0.9	0.9	−26.7	+23.9
		+0.2	**0.9**	**0.9**	**−26.1**	**+24.0**
30–40	8×10^6	−0.02	1.09	1.09	−23.9	+21.6
		+0.15	**1.08**	**1.09**	**−23.0**	**+22.2**
40–50	0[b]	—	—	—	—	—
50–60	4×10^6	+0.08	0.99	0.99	−11.9	+11.0
		+0.21	**1.00**	**1.02**	**−11.6**	**+11.8**
60–70	0[b]	—	—	—	—	—
70–80	0[b]	—	—	—	—	—
80–90	0[b]	—	—	—	—	—
90–100	0[b]	—	—	—	—	—
100–110	0[b]	—	—	—	—	—
110–120	0[b]	—	—	—	—	—

[a]Units are TECU; 400 km shell only. All times, all latitudes, all horizon angles. Statistics using the original $1/\cos(z')$ function are shown in nonbold type. Statistics using the new mapping function ($\hat{W}_{new}$) are shown in bold type.

[b]No days with an A_p value in this range occurred during the study period.

relative to the reliable results which seem to come from the 400 km shell choice.

[72] The final single-variable analysis was about the A_p index, in Table 9. What is decidedly odd about this table is that no immediate correlation between A_p index and E is obvious. However, as only 3 days had A_p indices above 30 (two in the 30–40 range, one in the 50–60 range) in this 5 month period, the amount of data is somewhat prohibitive. One possible interpretation is that as geomagnetic activity increases the ionosphere tends to become more "chemically" controlled, particularly in summer and equinox, which is the period under study [*Fuller-Rowell et al.*, 1996]. Increased chemical control from storm-time changes in the neutral atmosphere (thermosphere) tends to increase the rate of ion recombination, and hence decrease plasma densities. Variability from other sources, such as neutral wind surges, is also less effective during these times. The same study may indicate increased variability in winter as a function of A_p. It may also be the case that more severe geomagnetic disturbance will eventually reverse the apparent trend seen in Tables 9 and 10.

12. Combinations Yielding Best Performance

[73] It cannot be overemphasized that the reason 2-D shells have been used for so long is that there are significant advantages to them (smaller data storage, simpler mathematical formulation, easier dissemination over limited bandwidths, etc.). Recognizing this, and thus the likelihood that some applications will continue to use shell models indefinitely, it seems useful to ask what the very best performance one can obtain with a shell model might be. This means picking certain variables, of which the first choice seems obvious from the previous tables: use a shell height of 400 km. Focusing on that specifically, one can dig deeper for the optimal way to use a shell model. It is hypothesized that the lack of significant improvement in statistics with lower A_p values might have been clouded by the number of "bad shells" which went into that table. Looking exclusively at only the 400 km shell, Table 9 can be recalculated and is presented in Table 10.

[74] Unfortunately, and once again, these results are somewhat confusing and unsatisfying. No clear indication that a larger A_p value yields a lack of reliability in a shell model can be seen. Obviously more data are needed for days of greater ionosphere activity to draw reasonable conclusions. Furthermore, as already pointed out in Table 8, the new mapping function is not much of an aid to improvement when focusing solely on the 400 km shell.

[75] To further exemplify the usefulness of a shell model at 400 km, Table 7 was recreated only with the 400 km shell and presented in Table 11. That table shows the RMS for E values does not exceed 1.0 TECU until the raypath is as low as 20 degrees above the horizon. This is a definite improvement over the "all shells" statistics which Table 7 presented.

[76] Also, Table 11 allows a closer examination of the impact of switching to the new mapping function for this particular shell. Examining average, standard deviation and RMS values it can be seen that at the lowest horizon angles, the new mapping function actually has a very

Table 11. STEC – MSTEC by Angle Above the Horizon[a]

Horizon Angle	Number of Values	Average	Standard Deviation	RMS	Minimum	Maximum
0–5	41×10^6	+0.6	1.5	1.7	−26.7	+43.9
		+0.9	**1.5**	**1.8**	**−26.1**	**+44.2**
5–10	44×10^6	+0.3	1.4	1.4	−22.8	+25.9
		+0.6	**1.4**	**1.5**	**−22.2**	**+26.0**
10–15	44×10^6	+0.0	1.2	1.2	−20.0	+20.7
		+0.3	**1.1**	**1.2**	**−19.7**	**+20.8**
15–20	44×10^6	−0.2	1.0	1.0	−19.8	+16.3
		+0.1	**1.0**	**1.0**	**−18.5**	**+16.5**
20–25	43×10^6	−0.2	0.8	0.9	−20.9	+13.8
		+0.1	**0.8**	**0.8**	**−19.5**	**+14.7**
25–30	41×10^6	−0.2	0.7	0.8	−15.3	+12.5
		+0.1	**0.7**	**0.7**	**−14.1**	**+13.2**
30–35	40×10^6	−0.2	0.7	0.7	−14.9	+12.8
		+0.0	**0.6**	**0.6**	**−13.9**	**+13.2**
35–40	39×10^6	−0.1	0.6	0.6	−12.9	+11.9
		+0.0	**0.5**	**0.5**	**−12.4**	**+12.0**
40–45	36×10^6	−0.1	0.5	0.5	−11.6	+9.0
		+0.0	**0.5**	**0.5**	**−11.1**	**+9.0**
45–50	34×10^6	−0.1	0.4	0.4	−8.7	+9.3
		+0.0	**0.4**	**0.4**	**−8.4**	**+9.4**
50–55	30×10^6	−0.1	0.3	0.3	−9.5	+7.5
		+0.0	**0.3**	**0.3**	**−9.3**	**+7.6**
55–60	27×10^6	−0.05	0.3	0.3	−8.3	+7.3
		−0.00	**0.3**	**0.3**	**−8.1**	**+7.3**
60–65	23×10^6	−0.04	0.3	0.3	−6.7	+7.1
		−0.01	**0.3**	**0.3**	**−6.6**	**+7.1**
65–70	20×10^6	−0.02	0.2	0.2	−4.4	+5.3
		−0.00	**0.2**	**0.2**	**−4.3**	**+5.3**
70–75	16×10^6	−0.02	0.2	0.2	−5.2	+8.3
		−0.01	**0.2**	**0.2**	**−5.2**	**+8.3**
75–80	12×10^6	−0.01	0.2	0.2	−5.2	+4.9
		−0.00	**0.2**	**0.2**	**−5.2**	**+5.0**
80–85	8×10^6	−0.003	0.1	0.1	−2.9	+3.1
		−0.000	**0.1**	**0.1**	**−2.9**	**+3.1**
85–90	3×10^6	−0.002	0.2	0.2	−3.3	+3.6
		−0.002	**0.2**	**0.2**	**−3.3**	**+3.6**

[a]Units are TECU; 400 km shell only. All times, all latitudes, all A_p values. Statistics using the original $1/\cos(z')$ function are shown in nonbold type. Statistics using the new mapping function ($\hat{W}_{new}$) are shown in bold type.

slight degradation in the statistics. However, once the raypaths are more than 20 degrees above the horizon, the new mapping function yields a very slight improvement.

[77] Table 11 shows some good news for those applications which must rely on a shell model. Generally speaking, the use of a 400 km shell allows raypaths as low as 15 degrees above the horizon while maintaining an RMS accuracy of 1.0 TECU. The elimination of raypaths below 15 degrees only corresponds to 26% of all raypaths over these days. And if this additional data is needed (accompanied by an allowable loss of accuracy) the RMS never exceeds 1.7 TECU for this shell model.

[78] Generally speaking, if one is using a shell model, the only controllable variables are shell height and cutoff angle for raypaths. After that, most shell models must be expected to work at a variety of latitudes, and times of day. About the only case not strongly studied is that of very high geomagnetic activity, such as during geomagnetic storms. Further studies should focus exclusively on using shell models during more energetic ionospheric activity.

13. Conclusions

[79] This paper has focused on the errors inherent to the use of spherical shell models of the ionosphere. Such models, while simple to use, contain no information about the vertical structure of the ionosphere and therefore cannot perfectly describe the Total Electron Content of a ray whose path slants through the shell.

[80] It was shown that the frequently used "original mapping function" ($1/\cos(z')$) which connects the vertical TEC to the slant TEC is mathematically perfect if (and only if) the ionosphere truly is a spherical shell of zero thickness. However, a number of geometric examples were then used to examine how the original

mapping function fails even under the most simplistic of three-dimensional and horizontally uniform conditions.

[81] While none of the geometric examples was meant to capture a realistic vertical structure, they all showed that a stratified ionosphere (without any vertical mixing), cannot be perfectly captured using a shell model combined with the original mapping function. While the errors could be as small as a few tenths of a TECU, such a systematic error would propagate poorly in positioning applications which rely on a priori knowledge of the ionosphere.

[82] When quantifying the purely geometric error, an ''average stratification'' model was tested against shell models and a very simple pattern of geometric error was discerned. This simple pattern was dependent upon shell height and piercing angle. Upon studying this pattern of geometric error, a ''new mapping function'' $\hat{W}_{new}$ was proposed which scaled the ''original mapping function'' to remove the geometric error. It would be of value to test this function on other model ionospheres.

[83] An attempt to quantify the total error of using a shell model (combining both geometric issues with actual vertical and horizontal structure) was made by using the US-TEC model of NOAA's Space Weather Prediction Center. Seven months of US-TEC data were examined. Actual integrated TEC values along slant raypaths were compared against values mapped from the vertical TEC values using both the ''original'' and ''new'' mapping functions. The statistics of these STEC-MSTEC data were broken down five different ways, each based on a different variable: latitude, time of day, vertical angle, shell height and A_p index (ionosphere activity).

[84] Although the conclusions were mixed from the view of Ap index, the conclusion drawn from investigating latitude, time of day, vertical angle and shell height all were conclusive: improvements of 30% to 50% in matching mapped STEC to actually integrated STEC could be gained by switching from the original mapping function to the new mapping function.

[85] Additionally, these data helped answer whether an ''optimal shell model'' could be found was then addressed. Based on the results in this paper, the following conclusions could be drawn:

[86] 1. If one is using a shell at 400 km height, and data are restricted to 15 degrees or more above the horizon (and, ostensibly, has an A_p index of no more than 30) then the errors inherent in using a shell model can be contained to an RMS of 1.0 TECU. The new mapping function yielded smaller residuals in this case, but worked worse than the original mapping function below horizon angles of 15 degrees.

[87] 2. If any other shell height besides 400 km is used (for example, if using the WAAS ionosphere model which places the shell at 350 km) then using the new mapping function reduces disagreement between STEC and MSTEC by a factor as much as 50%.

[88] While the use of shell models will always contain some inherent error, it was shown that such error can be controlled by optimal choice of variables (specifically shell height, piercing angle and mapping function). If, however, one is interested in accuracies of the slant TEC which are always below 1.0 TECU, then no shell model could be found which satisfied this criteria, unless one were restricted to very nearly vertical raypaths, which seems too restrictive to be applied to most general purposes.

[89] This study exclusively examined the errors in a 2-D shell model. Further investigations could be done which examine the error inherent in using spherical, rather than the more accurate ellipsoidal, shapes for both the 2-D and 3-D ionosphere models.

Appendix A

[90] Equation (4) shows a concise relationship between r_b, r_t, r_s, z' and s. That relationship is derived in this appendix. Consider an expansion of Figure 1, as seen in Figure A1. One new detail is labeling the center of the r_b, r_s and r_t spheres as point ''O''. If the line through points A and B is radial, then the equation for ''s'' simplifies to the equation for ''d'' seen in equation (5). However, in the general case, the line through A and B is nonradial and can therefore be extended Earthward until it intersects with another radius, from O to F, forming a right angle at point F as shown. The actual size of ''r_f'' is unimportant, as it is only a computational tool which will eventually fall out of the equation for ''s''. It has no relationship with any other spheres mentioned in this paper, and is different for every combination of r_b, r_s, r_t and z'.

[91] Begin with the following simple relationship:

$$s = v - d \tag{A1}$$

[92] By the Pythagorean theorem applied first to triangle FOB and then to triangle FOA, the equations for v and d are:

$$v^2 + r_f^2 = r_t^2 \Rightarrow v = \sqrt{r_t^2 - r_f^2} \tag{A2}$$

$$d^2 + r_f^2 = r_b^2 \Rightarrow d = \sqrt{r_b^2 - r_f^2} \tag{A3}$$

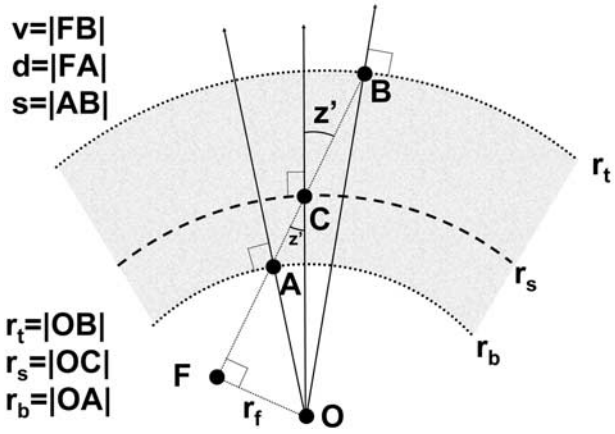

Figure A1. Expansion of ionosphere geometry for deriving equation (4).

[93] Substituting equations (A3) and (A2) into (A1), yields:

$$s = \sqrt{r_t^2 - r_f^2} - \sqrt{r_b^2 - r_f^2} \tag{A4}$$

[94] All that remains is to remove r_f from equation (A4). From the Sine law, applied to right triangle OFC:

$$\frac{r_f}{\sin z'} = \frac{r_s}{\sin 90^\circ} \tag{A5}$$

which, when rearranged, yields:

$$r_f = r_s \sin z' \tag{A6}$$

[95] Substituting equating equation (A6) into equation (A4) yields equation (4) in the main portion of the paper.

References

Araujo-Pradere, E. A., T. J. Fuller-Rowell, P. S. J. Spencer, and C. F. Minter (2007), Differential validation of the USTEC model, *Radio Sci.*, *42*, RS3016, doi:10.1029/2006RS003459.

Bilitza, D. (2001), International Reference Ionosphere 2000, *Radio Sci.*, *36*(2), 261–275.

Fuller-Rowell, T. J., M. V. Codrescu, H. Rishbeth, R. J. Moffet, and S. Quegan (1996), Response of the thermosphere and ionosphere to geomagnetic storms, *J. Geophys. Res.*, *101*, 2343–2353.

Fuller-Rowell, T. J., E. A. Araujo-Pradere, C. F. Minter, M. V. Codrescu, P. S. J. Spencer, D. Robertson, and A. R. Jacobson (2006), US-TEC: A new data assimilation product from the Space Environment Center characterizing the ionospheric total electron content using real-time GPS data, *Radio Sci.*, *41*, RS6003, doi:10.1029/2005RS003393.

Komjathy, A. (1997), Global ionospheric total electron content mapping using the Global Positioning System, Ph.D. dissertation, 248 pp., Dep. of Geod. and Geomatics Eng., Univ. of New Brunswick, Fredericton, New Brunswick, Canada.

Komjathy, A., and R. B. Langley (1996), An assessment of predicted and measured ionospheric total electron content using a regional GPS network, in *Proceedings of the National Technical Meeting of the Institute of Navigation*, pp. 615–624, Inst. of Navig., Alexandria, Va.

Minter, C. F., D. S. Robertson, P. S. J. Spencer, A. R. Jacobsen, T. J. Fuller-Rowell, E. A. Araujo-Pradere, and R. W. Moses (2007), A comparison of MAGIC and FORTE ionospheric measurements, *Radio Sci.*, *42*, RS3026, doi:10.1029/2006RS003460.

Radicella, S. M., B. Nava, P. Coisson, L. Kersley, and G. Bailey (2004), Effects of gradients of the electron density on Earth-space communications, *Ann. Geophys.*, *47*(suppl.), 1227.

Spencer, P. S. J., D. S. Robertson, and G. L. Mader (2004), Ionospheric data assimilation methods for geodetic applications, paper presented at IEEE PLANS 2004, Inst. of Electr. and Electron. Eng., Monterey, Calif., 26–29 April.

E. A. Araujo-Pradere, T. Fuller-Rowell, and C. Minter, Space Weather Prediction Center, National Oceanic and Atmospheric Administration, Boulder, CO 80305, USA.

D. A. Smith, National Geodetic Survey, National Oceanic and Atmospheric Administration, Silver Spring, MD 20910, USA. (dru.smith@noaa.gov)